COMPUTATIONAL STUDY OF THE DISPERSIVELY MODIFIED KURAMOTO–SIVASHINSKY EQUATION*

G. AKRIVIS†, D. T. PAPAGEORGIOU‡, AND Y.–S. SMYRLIS§

Abstract. We analyze and implement fully discrete schemes for periodic initial value problems for a general class of dispersively modified Kuramoto–Sivashinsky equations. Time discretizations are constructed using linearly implicit schemes and spectral methods are used for the spatial discretization. The general case analyzed covers several physical applications arising in multi-phase hydrodynamics and the emerging dynamics arise from a competition of long-wave instability (negative diffusion), short–wave damping (fourth order stabilization), nonlinear saturation (Burgers nonlinearity) and dispersive effects. The solutions of such systems typically converge to compact absorbing sets of finite dimension (i.e., global attractors) and are characterized by chaotic behavior. Our objective is to employ schemes which capture faithfully these chaotic dynamics. In the general case the dispersive term is taken to be a pseudo-differential operator which is allowed to have higher order than the familiar fourth order stabilizing term in Kuramoto–Sivashinsky equation. In such instances we show that first– and second–order time–stepping schemes are appropriate and provide convergence proofs for the schemes. In physical situations when the dispersion is of lower order than the fourth order stabilization term (for example a hybrid Kuramoto–Sivashinsky–Korteweg–deVries equation also known as the Kawahara equation in hydrodynamics), higher order time–stepping schemes can be used and we analyze and implement schemes of order six or less. We derive optimal order error estimates throughout and utilize the schemes to compute the long time dynamics and to characterize the attractors. Various numerical diagnostic tools are implemented, such as the projection of the infinite–dimensional dynamics to one–dimensional return maps that enable us to probe the geometry of the attractors quantitatively. Such results are only possible if computations are carried out for very long times (we provide examples where integrations are carried out for 10^8 time units), and it is shown that the schemes used here are very well suited for such tasks. For illustration, computations are carried out for third order dispersion (the Kawahara equation) as well as fifth order dispersion (the Benney–Lin equation) but the methods developed here are applicable for rather general dispersive terms with similar accuracy characteristics.

Key words. Dispersive–dissipative systems, Kuramoto–Sivashinsky equation, linearly implicit schemes, pseudo–spectral methods, chaotic attractors.

AMS subject classifications. Primary 65M60, 65M12; Secondary 65L06

1. Introduction.

We consider the periodic initial value problem for the dispersively modified Kuramoto–Sivashinsky (KS) equation

$$u_t + uu_x + u_{xx} + \nu u_{xxxx} + \mathcal{D}u \;=\; 0, \tag{1.1}$$

with $u = u(x,t)$ a $2\pi-$periodic function in the first variable, ν a positive constant and u^0 a given initial value,

$$u(\cdot,0) = u^0. \tag{1.2}$$

In (1.1), $\mathcal{D}$ is a dispersive linear pseudo–differential operator defined by

$$(\widehat{\mathcal{D}v})_\ell \;=\; \mathrm{i} f(\ell)\,\hat{v}_\ell,$$

†Computer Science Department, University of Ioannina, 451 10 Ioannina, Greece (akrivis@cs.uoi.gr).

‡Department of Mathematics, Imperial College London, London, SW7 2AZ, UK (d.papageorgiou@imperial.ac.uk).

§Department of Mathematics and Statistics, University of Cyprus, 1678 Nicosia, Cyprus (smyrlis@ucy.ac.cy).

*This work was supported by University of Cyprus grant #8037P-3/311-21028. The work of DTP was also supported by the National Science Foundation grant DMS-0707339.

with $\hat{v}_\ell$ the Fourier coefficients of v, $v(x) = \sum_{\ell\in\mathbb{Z}} \hat{v}_\ell \mathrm{e}^{\mathrm{i}\ell x}$, and f a given odd real-valued function, $f(-\ell) = -f(\ell)$. Let us note that, in the case of vanishing $\mathcal{D}$, equation (1.1) reduces to the well-known Kuramoto–Sivashinsky equation. In the absence of the Kuramoto–Sivashinsky terms (the second and fourth derivatives of u), equation (1.1) reduces to a dispersive equation which is analogous to the Korteweg–deVries (KdV) equation. Thus, the model considered here bridges two fundamental equations of applied mathematics and our objective is in the accurate and efficient computation of the dynamics of the hybrid system.

An equation of the form of (1.1) has been derived to describe the dynamics of core–annular film flows with applications to lubricated pipelining, in which case

$$f(\ell) \,=\, \frac{\ell^2 I_1(\ell)}{\ell I_1^2(\ell) - \ell I_0^2(\ell) + 2I_0(\ell)I_1(\ell)}, \tag{1.3}$$

and $I_p = I_p(\ell)$ denotes the modified Bessel function of the first kind of order p (see [16, 21]). Localized versions of (1.1) with $f(\ell)$ a cubic or quintic polynomial have also been derived in the context of viscous liquid films flowing down inclined planes (with applications in coating technologies, for instance). In the former case we obtain the so-called Kawahara equation

$$u_t + uu_x + u_{xx} + \delta_3 u_{xxx} + \nu u_{xxxx} \,=\, 0, \tag{1.4}$$

derived in [14, 19, 26], and note that the dispersive term is of lower order than the stabilizing term u_{xxxx}. Higher fifth order dispersion is retained in the equation

$$u_t + uu_x + u_{xx} + \delta_3 u_{xxx} + \nu u_{xxxx} + \delta_5 u_{xxxxx} \,=\, 0, \tag{1.5}$$

known as the Benney–Lin equation, which has been derived in the context of the one–dimensional evolution of sufficiently small amplitude long waves in various problems in fluid dynamics (see, for example, [8, 20]).

From an analytical perspective, the global well–posedness of the periodic initial value problem (1.1)–(1.2) is derived from [25]. For example, global well–posedness of the periodic initial value problem for (1.5) with initial data in $H^s_{\mathrm{per}}(\mathbb{R})$, $s \geq 0$, has been established in [10]; here, $H^s_{\mathrm{per}}(\mathbb{R})$ denotes the Sobolev space consisting of the $2\pi-$periodic functions with finite norm $\|v\|_{H^s}$; for the definition of this norm see (2.3) below. The boundedness of the solutions of (1.1) and the existence of compact attractors was proved in [15]; more specifically it was proved that the initial value problem possesses a maximal, connected, compact attractor in $H^s_{\mathrm{per}}(\mathbb{R})$ for any $s < 2$.

In [7], the modified KS equation (1.1) was rewritten in the form

$$u_t + \frac{1}{\nu}u + u_{xx} + \nu u_{xxxx} + \mathcal{D}u \,=\, \frac{1}{\nu}u - uu_x, \tag{1.6}$$

or, with the operators $\mathcal{L}$ and $\mathcal{B}$ given by

$$\mathcal{L}v \,=\, \Big(\frac{1}{\nu}v + v_{xx} + \nu v_{xxxx}\Big) + \mathcal{D}v, \quad \mathcal{B}(v) \,=\, \frac{1}{\nu}v - vv_x, \tag{1.7}$$

in the equivalent form

$$u_t + \mathcal{L}u \,=\, \mathcal{B}(u), \tag{1.8}$$

and its discretization in time by implicit–explicit multistep schemes was analyzed. The fact that the operator $\mathcal{L}$ can be split into $\mathcal{L} = \mathcal{A} + \mathcal{D}$, with $\mathcal{A}$,

$$\mathcal{A}v := \frac{1}{\nu}v + v_{xx} + \nu v_{xxxx}, \tag{1.9}$$

a symmetric and positive definite operator and $\mathcal{D}$ an antisymmetric operator, played a key role in the analysis in [7]. For a general dispersive operator $\mathcal{D}$, the dispersively modified KS equation can be stably discretized by $A-$stable schemes; hence, in particular, the highest attainable order by multistep schemes is two. Thus, we have chosen to discretize (1.1) by the implicit–explicit Euler and two-step BDF methods. In contrast, in case of low order dispersive operators like in the Kawahara equation (1.4), higher order time-stepping schemes may be stable, see [7]; due to this fact, we devote here a separate section to the discretization of the Kawahara equation.

One of our purposes is to combine the time stepping schemes with a pseudo-spectral method for the space discretization to construct and analyze fully discrete, implementable methods.

An outline of the paper is as follows: In Section 2 we consider the general case of the dispersively modified KS equation. We discretize in time by first– and second–order schemes and derive optimal error estimates. In subsection 2.4, as an example of low order dispersive terms, we focus on the special case of the Kawahara equation; in this case higher order time-stepping schemes may also be used. In all cases the spatial discretization is accomplished with a pseudo-spectral method. In Section 3, we briefly discuss issues of the numerical implementation of the schemes and in Section 4 present extensive results of the computational study of the dispersively modified KS equation. Finally, in Section 5 we summarize our conclusions.

2. Linearly implicit spectral schemes for dispersively modified KS equations. In this section we present the numerical schemes, first the time stepping schemes and subsequently the fully discrete schemes, and derive optimal order error estimates for equation (1.1). In subsection 2.4 we concentrate on equation (1.4).

2.1. Discretization in time by implicit–explicit multistep schemes. Let (α,β) and (α,γ) be implicit and explicit, respectively, $q-$step schemes, characterized by three polynomials α,β and γ,

$$\alpha(\zeta) = \sum_{i=0}^{q}\alpha_i\zeta^i, \quad \beta(\zeta) = \sum_{i=0}^{q}\beta_i\zeta^i, \quad \gamma(\zeta) = \sum_{i=0}^{q-1}\gamma_i\zeta^i.$$

Combining schemes (α,β) and (α,γ), we construct an implicit–explicit $(\alpha,\beta,\gamma)-$scheme for the discretization of equation (1.1), written in the form (1.8). Let $N\in\mathbb{N}$, $k:=T/N$ be the time step, $t^n:=nk$, $n=0,\dots,N$, and u the solution of (1.1)–(1.2). The linear part of equation (1.8) is discretized by the implicit scheme (α,β) and the nonlinear part by the explicit scheme (α,γ), i.e., we define approximations U^n to the values $u^n:=u(t^n):=u(\cdot,t^n)$ by the linearly implicit scheme

$$\sum_{i=0}^{q}\alpha_i U^{n+i} + k\sum_{i=0}^{q}\beta_i\mathcal{L}U^{n+i} = k\sum_{i=0}^{q-1}\gamma_i\mathcal{B}(U^{n+i}), \tag{2.1}$$

for given starting approximations $U^0,\dots,U^{q-1}$. In particular, we are interested in the implicit–explicit BDF schemes: For $q\in\{1,2,3,4,5,6\}$, let consider polynomials

$$\alpha(\zeta):=\sum_{j=1}^{q}\frac{1}{j}\zeta^{q-j}(\zeta-1)^j, \quad \beta(\zeta):=\zeta^q \quad \text{and} \quad \gamma(\zeta):=\zeta^q-(\zeta-1)^q.$$

The corresponding $(\alpha,\beta)-$scheme is the $q-$step BDF scheme; its order is $p=q$. These schemes are strongly $A(0)-$stable and, for $q=1,2$, $A-$stable. The order of

the explicit scheme (α,γ) is also $p=q$. In this case, scheme (2.1) reduces to

$$\sum_{i=0}^{q}\alpha_i U^{n+i}+k\mathcal{L}U^{n+q}=k\sum_{i=0}^{q-1}\gamma_i\mathcal{B}(U^{n+i}). \tag{2.2}$$

2.2. Discretization in space. For $s\in\mathbb{R}$ let $H^s(\mathbb{T})$ denote the Sobolev space of order s, consisting of the $2\pi-$periodic functions with norm

$$\|v\|_{H^s}\;=\;\Big(\sum_{\ell\in\mathbb{Z}}(1+\ell^2)^s\big|\hat v_\ell\big|^2\Big)^{1/2}, \tag{2.3}$$

whenever $v(x)=\sum_{\ell\in\mathbb{Z}}\hat v_\ell \mathrm{e}^{\mathrm{i}\ell x}$. The inner product in $H:=L^2(\mathbb{T})=H^0(\mathbb{T})$ is denoted by $(\cdot,\cdot)$, and the induced norm by $\|\cdot\|$. Let $|\!|\!|\cdot|\!|\!|$ denote the norm of the space $V=\mathscr{D}(\mathcal{A}^{1/2})$, defined by $|\!|\!|v|\!|\!|:=\|\mathcal{A}^{1/2}v\|$. We identify H with its dual, and denote by V' the dual of V, again by $(\cdot,\cdot)$ the duality pairing between V' and V, and by $|\!|\!|\cdot|\!|\!|_\star$ the dual norm on V', $|\!|\!|v|\!|\!|_\star:=\|\mathcal{A}^{-1/2}v\|$. Let $M\in\mathbb{N}$ and $S_M:=\operatorname{span}\{\varphi_{-M+1},\dots,\varphi_M\}$, with $\varphi_\ell(x):=\mathrm{e}^{\mathrm{i}\ell x}$. Let $P_M:V'\to S_M$ denote the orthogonal L^2-projection operator onto S_M, i.e., $(v-P_Mv,\chi)=0$, for all $\chi\in S_M$. If we expand $v\in L^2(\mathbb{T})$ in a Fourier series, $v=\sum_{\ell=-\infty}^{\infty}\hat v_\ell\,\varphi_\ell$, then P_Mv corresponds to the partial sum $P_Mv=\sum_{\ell=-M+1}^{M}\hat v_\ell\,\varphi_\ell$. Since differentiation commutes with P_M, we have $P_M\mathcal{L}=\mathcal{L}P_M$. Furthermore, we define the discrete nonlinear operator $\mathcal{B}_M:H^2(\mathbb{T})\to S_M$, $\mathcal{B}_M:=P_M\mathcal{B}$. In the *semidiscrete* problem corresponding to (1.1)–(1.2) we seek a function u_M, such that $u_M(t):=u_M(\cdot,t)\in S_M$, satisfying

$$\begin{cases}\partial_t u_M(t)+\mathcal{L}u_M(t)=\mathcal{B}_M(u_M(t)), & 0<t\le T,\\ u_M(0)=u_M^0,\end{cases} \tag{2.4}$$

with $u_M^0\in S_M$ a given approximation to u^0. To construct implementable, fully discrete schemes, we discretize the initial value problem (2.4) for a system of o.d.e's in time by the implicit–explicit $(\alpha,\beta,\gamma)-$scheme, i.e., we recursively define a sequence of approximations $U^\ell\in S_M$ to $u(t^\ell)$ by

$$\sum_{i=0}^{q}\alpha_i U^{n+i}+k\sum_{i=0}^{q}\beta_i\mathcal{L}U^{n+i}=k\sum_{i=0}^{q-1}\gamma_i\mathcal{B}_M(U^{n+i}). \tag{2.5}$$

2.3. Error estimates. Clearly, the operator $\mathcal{A}$ (see (1.9)) maps $H^4(\mathbb{T})$ into H, $\mathcal{A}:H^4(\mathbb{T})\to H$. Also, $\mathcal{A}$ is self-adjoint and positive definite operator,

$$(\mathcal{A}v,v)\;\ge\;\gamma|\!|\!|v|\!|\!|^2\quad\text{ for all } v\in V, \tag{2.6}$$

for an appropriate positive constant γ, with $V=H^2(\mathbb{T})$; cf. [6]. Furthermore, the operator $\mathcal{B}:V\to H$ satisfies the local Lipschitz condition

$$|\!|\!|\mathcal{B}(v)-\mathcal{B}(w)|\!|\!|_\star\;\le\;\mu\|v-w\|\quad\text{ for all } v,w\in T_u \tag{2.7}$$

in a tube T_u around the solution u defined in terms of the norm of H,

$$T_u\;:=\;\big\{v\in V\;:\;\min_{0\le t\le T}\|v-u(t)\|\le 1\big\}, \tag{2.8}$$

with (cf. [6])

$$\mu:=\frac{1}{\sqrt{\nu}}\Big[2\sqrt{\pi}\,\big(1+\max_{0\le t\le T}\|u(t)\|\big)+\sqrt{2}\Big]. \tag{2.9}$$

The projection $P_M : V' \to S_M$ has the following approximation property: For $m \in \mathbb{N}$, there exists a constant c, independent of v and M, such that, for $v \in H^m(\mathbb{T})$

$$\|v - P_M v\|_{H^\ell} \le cM^{\ell-m}\|v^{(m)}\|, \tag{2.10}$$

for $\ell = 0, \dots, m$ (cf. [9, 11]). Let $W(t) \in S_M$ denote the L^2-projection of $u(t)$ in $S_M, W(t) := P_M u(t)$, $t \in [0,T]$. Let $E_M(t) \in S_M$ denote the *consistency error* of the semidiscrete equation (2.4) for W,

$$E_M(t) := W_t(t) + \mathcal{L}W(t) - \mathcal{B}_M(W(t)), \quad t \in [0,T]. \tag{2.11}$$

It is readily seen that

$$E_M(t) \;=\; W_t(t) + P_M\mathcal{L}u(t) - P_M\mathcal{B}(W(t)),$$

and thus, in view of (1.8),

$$E_M(t) = P_M\big[\mathcal{B}(u(t)) - \mathcal{B}(W(t))\big].$$

To estimate $E_M(t) \in S_M$ we take here the inner product with $v \in S_M$ and obtain $(E_M(t), v) = (\mathcal{B}(u(t)) - \mathcal{B}(W(t)), v)$. Hence, we infer $|\!|\!| E_M(t) |\!|\!|_\star \le |\!|\!| \mathcal{B}(u(t)) - \mathcal{B}(W(t)) |\!|\!|_\star$. Therefore, in view of (2.7), $|\!|\!| E_M(t) |\!|\!|_\star \le \mu \|u(t) - W(t)\|$, and thus, using (2.10), we arrive at the desired optimal order estimate for the consistency error E_M,

$$\max_{0\le t\le T} |\!|\!| E_M(t) |\!|\!|_\star \le C(u)M^{-m} \quad \text{with} \quad \mathrm{C}(u) := c\mu \max_{0\le t\le T} \Big\| \frac{\partial^m u}{\partial x^m}(t) \Big\|. \tag{2.12}$$

Notice also that we immediately infer from (2.10) that $W(t) \in T_u$, for sufficiently large M.

Due to the presence of a dispersive operator $\mathcal{D}$ in equation (1.1), we assume that the scheme (α, β) is $A-$stable; this condition is needed for stability even in the case $\mathcal{B} = 0$ in (1.8). Consequently, according to the second Dahlquist barrier, the highest attainable order of the scheme (α, β) is two. Thus, in the remaining part of this subsection we consider one first order implicit–explicit scheme, namely the implicit–explicit Euler scheme, and one second order implicit–explicit scheme, namely the implicit–explicit two–step BDF scheme. The implicit–explicit Euler scheme for the semidiscrete problem (2.4) reads: Seek $U^\ell \in S_M$ such that

$$\begin{cases} U^{n+1} + k\mathcal{L}U^{n+1} \;=\; U^n + k\mathcal{B}_M(U^n), \quad n = 0, \dots, N-1, \\ U^0 = u_M^0. \end{cases} \tag{2.13}$$

To utilize the implicit–explicit two–step BDF scheme,

$$\frac{3}{2}U^{n+2} - 2U^{n+1} + \frac{1}{2}U^n + k\mathcal{L}U^{n+2} \;=\; 2k\mathcal{B}_M(U^{n+1}) - k\mathcal{B}_M(U^n) \tag{2.14}$$

we let $U^0 = u_M^0$, perform one step with the implicit–explicit Euler scheme to compute U^1, and let the approximations $U^2, \dots, U^N$ be given by the implicit–explicit BDF scheme. We can now derive optimal order error esimates:

THEOREM 2.1 (Error estimates). *Let $m \in \mathbb{N}$ and assume that the starting approximations U^0 is such that*

$$\|u^0 - U^0\| \le cM^{-m}. \tag{2.15}$$

Assume that the solution u of (1.1)–(1.2) *is sufficiently smooth such that $C(u)$ be finite; see* (2.12)*. Furthermore, we suppose that u is sufficiently smooth such that*

$$\sup_{0<t<T} |||u_{tt}(t)|||_\star \quad \textit{and} \quad \sup_{0<t<T} \|u_t(t)\|$$

in the case of the scheme (2.13)*, and*

$$\sup_{0<t<T} |||u_{ttt}(t)|||_\star \quad \textit{and} \quad \sup_{0<t<T} \Big|\Big|\Big| \frac{\partial^2 \mathcal{B}(u(t))}{\partial t^2} \Big|\Big|\Big|_\star$$

in the case of the scheme (2.14)*, respectively, are finite. Let $U^n \in S_M, n = 1, \dots, N$, be recursively defined by* (2.13) *or by* (2.14)*, respectively. Then, there exists a constant C, independent of k and M, such that, for k sufficiently small and M sufficiently large,*

$$\max_{0\le n\le N} \|u(t^n) - U^n\| \le C(k + M^{-m}), \tag{2.16}$$

if the approximations are computed by (2.13)*, and*

$$\max_{0\le n\le N} \|u(t^n) - U^n\| \le C(k^2 + M^{-m}), \tag{2.17}$$

if the approximations are computed by (2.14)*.*

Proof. We shall prove only the estimate (2.17); the proof of (2.16) goes along the same lines. Let $\tilde W^0 := W(\cdot, 0)$, and define $\tilde W^n \in S_M, n = 1, \dots, N$, by applying one step of the implicit–explicit Euler scheme and subsequently the implicit–explicit BDF2 scheme, cf. (2.14), to equation (2.11), i.e., by

$$\begin{cases} \tilde W^1 + k\mathcal{L}\tilde W^1 \;=\; \tilde W^0 + k\big[\mathcal{B}_M(\tilde W^0) + E_M(t^0)\big], \\ \dfrac{3}{2}\tilde W^{n+2} - 2\tilde W^{n+1} + \dfrac{1}{2}\tilde W^n + k\mathcal{L}\tilde W^{n+2} \;=\; 2k\big[\mathcal{B}_M(\tilde W^{n+1}) + E_M(t^{n+1})\big] \\ \qquad\qquad -k\big[\mathcal{B}_M(\tilde W^n) + E_M(t^n)\big], \quad n = 0, \dots, N-2. \end{cases} \tag{2.18}$$

Then, according to Proposition 3.1 of [7], we have

$$\max_{0\le n\le N} \|W(t^n) - \tilde W^n\| \le Ck^2. \tag{2.19}$$

In view of (2.10) and (2.19), it remains to estimate $\vartheta^n := \tilde W^n - U^n$. Now, since on the right-hand side of the local Lipschitz condition (2.7) only the norm $\|\cdot\|$ appears, i.e., in the notation of [7] we have $\lambda = 0$, we may use the stability estimate of Remark 3.2 of [7] to estimate ϑ^n. Indeed, subtracting (2.14) from (2.18), we conclude that

$$\|\vartheta^n\|^2 + k|||\vartheta^n|||^2 \le c\Big[\|\vartheta^0\|^2 + k\sum_{\ell=0}^{n-1} |||E_M(t^\ell)|||_\star^2\Big]. \tag{2.20}$$

From this estimate, (2.12) and (2.15), we easily conclude, for k sufficiently small and M sufficiently large,

$$\max_{0\le n\le N} \|\tilde W^n - U^n\| \le C(k^2 + M^{-m}). \tag{2.21}$$

From (2.10), (2.19) and (2.21) the desired estimate (2.17) follows. □

REMARK 2.1. Here we shall justify the regularity requirements in Theorem 2.1. First, obviously, the boundedness of $C(u)$ is needed in the estimate (2.12). Furthermore, in the case of the implicit–explicit Euler scheme, with E^n denoting its consistency error in the case of discretization in time only, see (2.2) for $q = 1$, we have

$$kE^n = u^{n+1} + k\mathcal{L}u^{n+1} - u^n - k\mathcal{B}(u^n).$$

Using the differential equation (1.8), we rewrite this relation in the form

$$\begin{aligned} kE^n &= u^{n+1} - u^n - ku_t(t^{n+1}) + k\big[\mathcal{B}(u^{n+1}) - \mathcal{B}(u^n)\big] \\ &= -\int_{t^n}^{t^{n+1}} (s - t^n)u_{tt}(s)\,ds + k\big[\mathcal{B}(u^{n+1}) - \mathcal{B}(u^n)\big]. \end{aligned}$$

Therefore, in view of the local Lipschitz condition (2.7),

$$\begin{aligned} k|\!|\!|E^n|\!|\!|_\star &\le \int_{t^n}^{t^{n+1}} (s - t^n)|\!|\!|u_{tt}(s)|\!|\!|_\star\,ds + \mu k\|u^{n+1} - u^n\| \\ &\le \int_{t^n}^{t^{n+1}} (s - t^n)|\!|\!|u_{tt}(s)|\!|\!|_\star\,ds + \mu k\int_{t^n}^{t^{n+1}} \|u_t(s)\|\,ds, \end{aligned}$$

and thus, under our smoothness assumptions, we infer that the following optimal order consistency estimate is valid

$$\max_{0\le n\le N-1} |\!|\!|E^n|\!|\!|_\star \le Ck.$$

Analogously, in the case of the implicit–explicit two–step BDF scheme, using the representation of the consistency error of [7, p. 156], we infer, under our smoothness assumptions, that the following optimal order consistency estimate is valid

$$\max_{0\le n\le N-1} |\!|\!|E^n|\!|\!|_\star \le Ck^2.$$

2.4. The Kawahara equation. In this section we consider the periodic initial value problem for the Kawahara equation (1.4), in which the dispersive term is of order lower than the one of $\mathcal{A}$, which allows us to use higher order implicit–explicit multistep schemes, as we shall see. First, we write the equation in the form

$$u_t + \frac{1}{\nu}u + u_{xx} + \nu u_{xxxx} = \frac{1}{\nu}u - \delta_3 u_{xxx} - uu_x. \tag{2.22}$$

Thus, with the operator $\mathcal{A}$ given in (1.9) and the nonlinear operator $\tilde{\mathcal{B}}$,

$$\tilde{\mathcal{B}}(v) := \frac{1}{\nu}v - \delta_3\, v_{xxx} - vv_x, \tag{2.23}$$

the Kawahara equation takes the form

$$u_t + \mathcal{A}u = \tilde{\mathcal{B}}(u). \tag{2.24}$$

Let us recall from [7] that

$$|\!|\!|\tilde{\mathcal{B}}(v) - \tilde{\mathcal{B}}(\tilde{v})|\!|\!|_\star \le \varepsilon|\!|\!|v - \tilde{v}|\!|\!| + C_\varepsilon\|v - \tilde{v}\| \quad \text{for all } v, \tilde{v} \in T_u, \tag{2.25}$$

with the tube T_u as in (2.8), for any positive ε and a constant C_ε depending on δ_3, ε and $\max_{0\le t\le T}\|u(t)\|$. Thus, all linearly implicit schemes of [1], and, in particular, the implicit–explicit $q-$step BDF schemes, with $q = 1,\dots,6$, see [6], are locally stable for (2.24) and consequently suitable for the discretization of (1.4). We will use the notation introduced in the previous section. Furthermore, we let the operator $\tilde{\mathcal{B}}_M$ be given by $\tilde{\mathcal{B}}_M := P_M\tilde{\mathcal{B}}$; see (2.23). In the *semidiscrete* problem corresponding to the periodic initial value problem (1.4) with (1.2) we seek a function $u_M(t) \in S_M$, satisfying

$$\begin{cases} \partial_t u_M(t) + \mathcal{A}u_M(t) = \tilde{\mathcal{B}}_M(u_M(t)), \quad 0 < t \le T, \\ u_M(\cdot,0) = u_M^0, \end{cases} \tag{2.26}$$

with $u_M^0 \in S_M$ a given approximation to u^0. Let $W(t)\in S_M$ denote the L^2-projection of $u(t)$ in S_M, $W(t) = P_M u(t)$, $t\in[0,T]$. Let $\tilde{E}_M(t)\in S_M$ denote the *consistency error* of the semidiscrete equation (2.26) for W,

$$\tilde{E}_M(t) := W_t(t) + \mathcal{A}W(t) - \tilde{\mathcal{B}}_M(W(t)), \quad t \in [0,T]. \tag{2.27}$$

Clearly, with $\mathcal{L}v := \mathcal{A}v + \delta_3\, v_{xxx}$,

$$\tilde{E}_M(t) = W_t(t) + P_M\mathcal{L}u(t) - P_M\mathcal{B}(W(t)),$$

and the consistency estimate

$$\max_{0\le t\le T} |\!|\!| \tilde{E}_M(t) |\!|\!|_\star \le C(u)M^{-m} \tag{2.28}$$

is a particular case of the more general result (2.12). We discretize the initial value problem (2.26) for a system of o.d.e's in time by an implicit–explicit $(\alpha,\beta,\gamma)-$scheme, i.e., we recursively define a sequence of approximations $U^\ell \in S_M$ to $u(t^\ell)$ by

$$\sum_{i=0}^{q} \alpha_i U^{n+i} + k\sum_{i=0}^{q} \beta_i \mathcal{A}U^{n+i} = k\sum_{i=0}^{q-1} \gamma_i \tilde{\mathcal{B}}_M(U^{n+i}), \tag{2.29}$$

$i = 0,\dots,N-q$, for given starting approximations $U^0,\dots,U^{q-1}\in S_M$. We assume that the implicit scheme (α,β) is strongly $A(0)-$stable and let p be the order of both schemes (α,β) and (α,γ); see [2] and [3]. Then, we have the following error estimate:

Proposition 2.2 (Error estimates). *Let $m\in\mathbb{N}$ and assume that the starting approximations $U^0,\dots,U^{q-1}$ are such that*

$$\max_{0\le j\le q-1} \left(\|W^j - U^j\| + \sqrt{k}\, |\!|\!| W^j - U^j |\!|\!| \right) \le c(k^p + M^{-m}). \tag{2.30}$$

Assume that the solution u of (1.4)–(1.2) is sufficiently smooth such that $C(u)$ (see (2.12)),

$$\sup_{0<t<T} |\!|\!| \frac{\partial^{p+1}u}{\partial t^{p+1}}(t) |\!|\!|_\star \quad \text{and} \quad \sup_{0<t<T} \left\| \frac{\partial^{p+2}u}{\partial t^p\,\partial x^2}(t) \right\|$$

be finite. Let $U^n\in S_M$, $n = q,\dots,N$, be recursively defined by (2.29). Then, if the solution u of (1.4)–(1.2) is sufficiently smooth, there exists a constant C, independent of k and M, such that, for k sufficiently small and M sufficiently large,

$$\max_{0\le n\le N} \|u(t^n) - U^n\| \le C(k^p + M^{-m}). \tag{2.31}$$

Proof. Let $\tilde{W}^j := W(t^j), j = 0, \dots, q-1$, and define $\tilde{W}^n \in S_M, n = q, \dots, N$, by applying the implicit–explicit $(\alpha, \beta, \gamma)-$scheme to equation (2.27), i.e., by

$$\sum_{i=0}^{q} \alpha_i \tilde{W}^{n+i} + k \sum_{i=0}^{q} \beta_i \mathcal{A} \tilde{W}^{n+i} = k \sum_{i=0}^{q-1} \gamma_i \big[\tilde{\mathcal{B}}_M(\tilde{W}^{n+i}) + \tilde{E}_M(t^{n+i}) \big], \tag{2.32}$$

$i = 0, \dots, N-q$. Then, according to Theorem 4.1 of [1] (see, also, [3]), we have

$$\max_{0 \le n \le N} \|W(t^n) - \tilde{W}^n\| \le C k^p. \tag{2.33}$$

In view of (2.10) and (2.33), it remains to estimate $\vartheta^n := \tilde{W}^n - U^n$. Subtracting (2.29) from (2.32) and using the stability estimate (4.6) of [1], we conclude that

$$\|\vartheta^n\|^2 + k \sum_{\ell=0}^{n} |\!|\!| \vartheta^\ell |\!|\!|^2 \le c \Big[\sum_{j=0}^{q-1} \big(\|\vartheta^j\|^2 + k |\!|\!| \vartheta^j |\!|\!|^2 \big) + k \sum_{\ell=0}^{n-q} |\!|\!| \tilde{E}_M(t^\ell) |\!|\!|_\star^2 \Big]. \tag{2.34}$$

From this estimate, (2.28) and (2.30), we easily conclude, for k sufficiently small and M sufficiently large,

$$\max_{0 \le n \le N} \|\tilde{W}^n - U^n\| \le C(k^p + M^{-m}). \tag{2.35}$$

From (2.10), (2.33) and (2.35) the desired estimate (2.31) follows. □

Remark 2.2. Here we shall justify the regularity requirements in Proposition 2.2. First, obviously, the boundedness of $C(u)$ is needed in the estimate (2.28). Furthermore, the consistency error of the $(\alpha, \beta, \gamma)-$scheme for equation (2.24) in the case of discretization in time only, cf. (2.29), is given by

$$kE^n = \sum_{i=0}^{q} \alpha_i u^{n+i} + k \sum_{i=0}^{q} \beta_i \mathcal{A} u^{n+i} - k \sum_{i=0}^{q-1} \gamma_i \tilde{\mathcal{B}}(u^{n+i}).$$

Using here the differential equation (2.24), Taylor expanding around t^n and using the order properties of the schemes (α, β) and (α, γ), we easily see that

$$\begin{aligned} kE^n = {} & \frac{1}{p!} \sum_{i=0}^{q} \int_{t^n}^{t^{n+i}} (t^{n+i} - s)^{p-1} \big[\alpha_i (t^{n+i} - s) - pk\beta_i \big] \frac{\partial^{p+1} u}{\partial t^{p+1}}(s)\, ds \\ & + \frac{k}{(p-1)!} \sum_{i=0}^{q} (\beta_i - \gamma_i) \int_{t^n}^{t^{n+i}} (t^{n+i} - s)^{p-1} \mathcal{A} \frac{\partial^p u}{\partial t^p}(s)\, ds, \end{aligned}$$

with $\gamma_q = 0$. Therefore, under our smoothness assumptions, we infer that the following optimal order consistency estimate is valid

$$\max_{0 \le n \le N-1} |\!|\!| E^n |\!|\!|_\star \le C k^p.$$

Remark 2.3. The $q-$step implicit–explicit BDF schemes, $q = 1, \dots, 6$, satisfy the conditions of Proposition 2.2 and their order is $p = q$. For $q = 1$ and $q = 2$, both

Theorem 2.1 and Proposition 2.2 apply for the Kawahara equation. We emphasize that the schemes in this and the previous subsection do not coincide; indeed, here the dispersive term is discretized explicitly while in the previous subsection it is discretized implicitly. Also, the condition (2.30) on the starting approximations in Proposition 2.2 is stronger than the corresponding condition (2.15) in Theorem 2.1.

REMARK 2.4. The results of this subsection can be easily extended to the general class of linearly implicit schemes considered in [1].

3. Numerical implementation. In our analysis of the implicit–explicit BDF schemes that approximate solutions of equation (1.1), we worked with an equation of the form $u_t + \mathcal{L}u = \mathcal{B}(u)$, with the operators $\mathcal{L}$ and $\mathcal{B}$ of (1.7). We consider spatially $2\pi-$periodic solutions and express u as

$$u(x,t) \,=\, \sum_{j\in\mathbb{Z}} \hat{u}_j(t)\, \mathrm{e}^{\mathrm{i}jx} \,=\, \frac{1}{2}a_0 + \sum_{j=1}^{\infty} \big(a_j(t)\, \cos jx + b_j(t)\, \sin jx\big). \tag{3.1}$$

The coefficient a_0 is constant due to the conservative nature of (1.1), and is taken to be zero (without loss of generality) by Galilean invariance. The nonlinear term $-uu_x$ is expressed as

$$-u(x,t)u_x(x,t) \,=\, \sum_{j\in\mathbb{Z}} \hat{f}_j(t)\, \mathrm{e}^{\mathrm{i}jx} \,=\, \sum_{j=1}^{\infty} \big(A_j(t)\, \cos jx + B_j(t)\, \sin jx\big), \tag{3.2}$$

where, for $j\in\mathbb{N}$,

$$\begin{aligned} A_j(t) \,&=\, -\frac{j}{2} \sum_{k+\ell=j} a_k b_\ell + \frac{j}{2} \sum_{k-\ell=j} (a_k b_\ell - a_\ell b_k), \\ B_j(t) \,&=\, \frac{j}{4} \sum_{k+\ell=j} (a_k a_\ell - b_\ell b_k) + \frac{j}{2} \sum_{k-\ell=j} (a_k a_\ell - b_\ell b_k). \end{aligned}$$

The dispersive term $\mathcal{D}$ in Fourier space diagonalizes as $\big(\widehat{\mathcal{D}u}\big)_j = d_j\, \hat{u}_j,\ \ j\in\mathbb{Z}$, where $d_j \in \mathbb{R}$ is the symbol of the operator $\mathcal{D}$, $d_{-j} = -d_j$, and from (3.1) it follows that

$$\mathcal{D}u(x,t) \,=\, \sum_{j=1}^{\infty} d_j \big(b_j(t)\, \cos jx - a_j(t)\, \sin jx\big).$$

Also (since u is real), $\hat{u}_j(t) \,=\, \frac{1}{2}\big(a_j(t) - \mathrm{i}b_j(t)\big)$ and $\hat{f}_j(t) \,=\, \frac{1}{2}\big(A_j(t) - \mathrm{i}B_j(t)\big)$. Replacing the operators $\mathcal{L}$ and $\mathcal{B}$, according to (1.7), in the implicit–explicit two–step BDF scheme (2.14) we obtain

$$\begin{aligned} &\Big(\frac{3}{2} + \frac{k}{\nu} + k\partial_x^2 + k\nu\partial_x^4 + \mathrm{i}k\mathcal{D}\Big)U^{n+2} \,= \\ &\Big(2 + \frac{2k}{\nu}\Big)U^{n+1} - \Big(\frac{1}{2} + \frac{k}{\nu}\Big)U^n - 2kU^{n+1}U_x^{n+1} + kU^nU_x^n, \end{aligned} \tag{3.3}$$

which in Fourier space takes the form

$$\begin{aligned} \hat{U}_j^{n+2} =& \frac{\Big(2 + \frac{2k}{\nu}\Big)(\xi_j - \mathrm{i}kd_j)}{\xi_j^2 + k^2d_j^2}\hat{U}_j^{n+1} - \frac{\Big(\frac{1}{2} + \frac{k}{\nu}\Big)(\xi_j - \mathrm{i}kd_j)}{\xi_j^2 + k^2d_j^2}\hat{U}_j^n \\ &+ \frac{2k(\xi_j - \mathrm{i}kd_j)}{\xi_j^2 + k^2d_j^2}\hat{F}_j^{n+1} - \frac{k(\xi_j - \mathrm{i}kd_j)}{\xi_j^2 + k^2d_j^2}\hat{F}_j^n, \end{aligned} \tag{3.4}$$

where $\xi_j = \frac{3}{2} + \frac{k}{\nu} - kj^2 + k\nu j^4$, with $\hat{U}_j^m$ the Fourier coefficients of the approximation U^m. Separating (3.4) into real and imaginary parts, with $\hat{U}_j^m = a_j^m - \mathrm{i}b_j^m$ and $\hat{F}_j^m = A_j^m - \mathrm{i}B_j^m$, gives the second order scheme

$$
\begin{aligned}
a_j^{n+2} =& \frac{\xi_j\left(2+\frac{2k}{\nu}\right)}{\xi_j^2+k^2d_j^2}a_j^{n+1} - \frac{kd_j\left(2+\frac{2k}{\nu}\right)}{\xi_j^2+k^2d_j^2}b_j^{n+1} - \frac{\xi_j\left(\frac{1}{2}+\frac{k}{\nu}\right)}{\xi_j^2+k^2d_j^2}a_j^{n} + \frac{kd_j\left(\frac{1}{2}+\frac{k}{\nu}\right)}{\xi_j^2+k^2d_j^2}b_j^{n} \\
&+ \frac{2k\xi_j}{\xi_j^2+k^2d_j^2}A_j^{n+1} - \frac{2k^2d_j}{\xi_j^2+d_j^2}B_j^{n+1} - \frac{k\xi_j}{\xi_j^2+k^2d_j^2}A_j^{n} + \frac{k^2d_j}{\xi_j^2+k^2d_j^2}B_j^{n}, \\
b_j^{n+2} =& \frac{kd_j\left(2+\frac{2k}{\nu}\right)}{\xi_j^2+k^2d_j^2}a_j^{n+1} + \frac{\xi_j\left(2+\frac{2k}{\nu}\right)}{\xi_j^2+k^2d_j^2}b_j^{n+1} - \frac{kd_j\left(\frac{1}{2}+\frac{k}{\nu}\right)}{\xi_j^2+k^2d_j^2}a_j^{n} - \frac{\xi_j\left(\frac{1}{2}+\frac{k}{\nu}\right)}{\xi_j^2+k^2d_j^2}b_j^{n} \\
&+ \frac{2k^2d_j}{\xi_j^2+k^2d_j^2}A_j^{n+1} + \frac{2k\xi_j}{\xi_j^2+k^2d_j^2}B_j^{n+1} - \frac{k^2d_j}{\xi_j^2+k^2d_j^2}A_j^{n} - \frac{k\xi_j}{\xi_j^2+k^2d_j^2}B_j^{n},
\end{aligned}
\tag{3.5}
$$

where $j \in \mathbb{N}$. Analogous formulæ for the implicit–explicit $q-$step BDF scheme, where $q = 1, 3, 4, 5, 6,$ may be found in [5].
In our space discretization, we project the solution onto the finite dimensional space $S_M = \left\{\mathrm{e}^{\mathrm{i}\ell x} : \ell = -M+1, \ldots, M\right\}$, where M is a suitably chosen integer. The justification of finite–dimensional truncations stems from the global boundedness of the Sobolev norms $H^s_{\mathrm{per}}(\mathbb{R})$, $s \leq 2$ (see [15]), which establish that the sequence $\{\omega_j\}_{j\in\mathbb{N}}$

$$
\omega_j \;=\; \limsup_{t\to+\infty} \left(a_j^2 + b_j^2\right)^{\frac{1}{2}}, \quad j \in \mathbb{N},
$$

decays faster than j^{-1}. Clearly such analytical estimates are not sharp and from a practical point of view the number of determining modes in the presence of dispersion is determined by numerical experimentation. Our extensive numerical experiments reveal that $\omega_j = \mathcal{O}(\mathrm{e}^{-\beta j})$, where the strip of analyticity β depends on ν and the dispersion. As we shall verify numerically in Section 4, for the specific cases of the Kawahara (1.4) and Benney–Lin (1.5) equations $\beta = \mathcal{O}(\nu^{1/2})$, as ν tends to zero, for any amount of dispersion.

4. Numerical experiments. In this section we present the results of extensive numerical experiments obtained by implemention of the schemes analyzed in Section 2. We have found that these schemes are both accurate and efficient when used for the numerical approximation of solutions to dispersive–dissipative equations like the ones studied here (many physical models fall in this class of evolution PDEs; see [7]).

In such types of equations it is important to carry out large time computations in order to establish the presence of attractors and quantify their characteristics in the presence of dispersion. To fix matters we consider the Benney–Lin equation (1.5), which has the advantage of retaining dispersive terms not dominated by the usual fourth order dissipation term of the KS equation. However, the presence of high order dispersion (fifth order in our case) restricts us to using first or second order implicit–explicit BDF schemes. On the other hand, the Kawahara equation (1.4), where only third–order dispersion is present, can be stably discretized by implicit–explicit BDF schemes of order up to six (numerical experiments showing the predicted theoretical accuracy are presented later).

4.1. Preliminary runs.

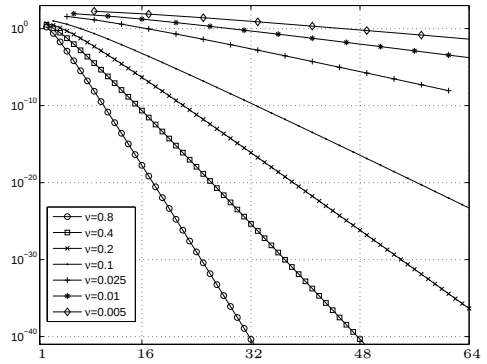

(a) Spectra of solutions of (1.4).

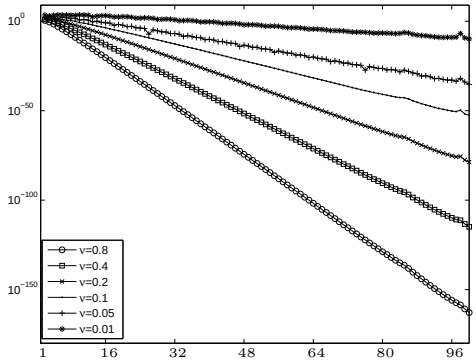

(b) Spectra of solutions of (1.5).

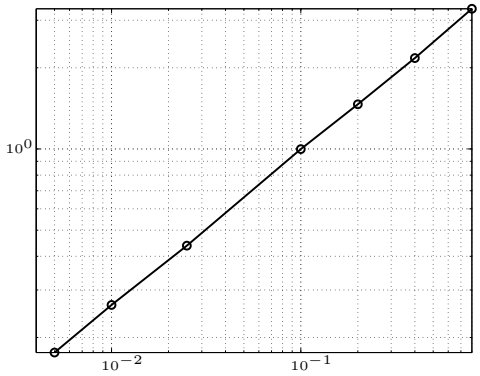

(c) Exponential decay rate variation with ν from (a).

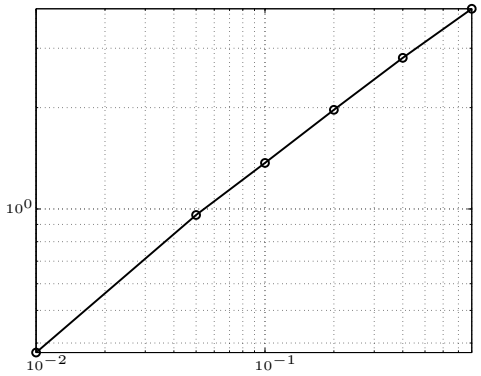

(d) Exponential decay rate variation with ν from (b).

FIG. 4.1. *Decay of Fourier coefficients as ν decreases. Kawahara equation* (1.4) *with $\delta_3 = 1$, panels* (a) *and* (c)*; Benney-Lin equation* (1.5) *with $\delta_3 = 0$, $\delta_5 = 1/2$, panels* (b) *and* (d)*. Panels* (a) *and* (b) *show log-linear plots of the spectrum of the solution and the values of ν are given in the figures. Panels* (c) *and* (d) *are logarithmic plots of the slopes of the spectra* (*i.e., the exponential decay rate at large wavenumbers*) *in* (a) *and* (b)*, respectively, estimated using a least squares fit, against ν; in both cases a power law ν^q is predicted with $q \approx 1/2$.*

Decay of Fourier modes. We have carried out numerical experiments in order to quantify the number of determining modes that contribute numerically to the solution. To fix matters, we consider the separate cases of vanishing δ_5 ($\delta_3 \neq 0$) or vanishing δ_3 ($\delta_5 \neq 0$) in equation (1.5). The results are shown in Figures 4.1(a)-4.1(d). Panels 4.1(a) and 4.1(b) depict the decay of the Fourier coefficients as ν decreases for the two cases (i) $\delta_3 = 1, \delta_5 = 0$, and (ii) $\delta_3 = 0, \delta_5 = 1/2$; both plots are log-linear with the Fourier wavenumber on the abscissæ and $\ln|\hat{u}_j|$ on the ordinates, where $|\cdot|$ denotes the modulus. Here $\hat{u}_j(t)$ are the Fourier coefficients of the solution and depend on t; spectral plots such as the ones in Figures 4.1(a)–4.1(b) were obtained by integrating to a sufficiently large time to ensure that the dynamics enter the attractor, and then taking a time average of the spectra over a prescribed time interval (typical length $5 - 10$ time units), or at the final time of integration. We observed that the high wavenumber behavior of the resulting plots are essentially the same and lead to identical conclusions regarding the analyticity of the solutions

– in Figures 4.1(a)–4.1(d) we provide spectra from the final computed times. The results provide conclusive evidence that the decay is exponential and of the form $|\hat{u}_j| = \mathcal{O}(\mathrm{e}^{-\beta(\nu)|j|})$. A least squares linear regression was used to estimate $\beta(\nu)$ for each of the curves in these two panels (typically regression over the modes $40 \le j \le 80$ was used; extending the range to higher values of j produces the same conclusions). The results are given in Tables 4.1 and 4.2 and also depicted using log-log coordinates in panels 4.1(c) and 4.1(d) for cases (i) and (ii), i.e., vanishing and non-vanishing δ_5 runs, respectively. We find strong evidence that $\beta(\nu) \sim \nu^q$, and the exponent q has been estimated using least squares regression to obtain the values 0.57 and 0.54 for cases (i) and (ii), respectively. Our numerical experiments indicate, therefore, that $\beta(\nu) \sim \nu^{1/2}$, a result that has been found numerically for the Kuramoto–Sivashinsky equation and related systems in the absence of dispersion (see [4, 12]).

ν	0.8	0.4	0.2	0.1	0.025	0.01	0.005
β	3.31	2.17	1.46	0.999	0.438	0.264	0.176
$\beta\nu^{-1/2}$	3.70	3.43	3.27	3.16	2.77	2.64	2.49

TABLE 4.1

The least squares estimates of the decay rate β from the runs of Figure 4.1(a), with $\delta_3 = 1$ and $\delta_5 = 0$. The last row indicates that $\beta(\nu) = \mathcal{O}(\nu^{1/2})$.

ν	0.8	0.4	0.2	0.1	0.05	0.01
β	3.93	2.81	1.97	1.37	0.96	0.388
$\beta\nu^{-1/2}$	4.39	4.44	4.41	4.33	4.30	3.88

TABLE 4.2

The least squares estimates of the decay rate β from the runs of Figure 4.1(b), with $\delta_3 = 0$ and $\delta_5 = 1/2$. The last row indicates that $\beta(\nu) = \mathcal{O}(\nu^{1/2})$.

The conclusion from these runs is that the solution can be computed with a finite number of Fourier modes. As an approximate and practical rule of thumb, in our experiments the size of the truncation is a small multiple of $\nu^{-1/2}$, e.g., $N = 4[\nu^{-1/2}]$. There is an interplay between the value of N and the size of the time–step required to maintain relative accuracy in the computation of the highest frequencies in the truncation. Such issues have been fully accounted for in all computational results presented here.

Accuracy of computed characteristics of the attractors. In the class of dissipative dynamical systems investigated here, our main interest is the prediction and quantification of the long time dynamics, which enable us to construct a picture of the global attractors. Hence, it is important to use schemes which maintain stability and accuracy over very long times. In Figure 4.2, for example, which depicts the foliations in a return map of a chaotic attractor, it was necessary to integrate to at least $T = 4 \times 10^4$ time units with a time step $k = 10^{-4}$. Table 4.3 shows the effect of the time-step and the order $p = q$ of the implicit–explicit $q-$step BDF scheme, $q = 1, \ldots, 6$, for time steps $k = (16, 8, 4, 2, 1) \times 10^{-4}$, when $\nu = 1/2$, $\delta_3 = 1$ and

k	16×10^{-4}	8×10^{-4}	4×10^{-4}	2×10^{-4}	10^{-4}
	Energy				
$p=1$	9.54606134	9.55217514	9.55522645	9.55675069	9.55751247
$p=2$	9.55827155	9.55827339	9.55827385	9.55827397	9.55827399
$p=3$	9.45762169	9.50677972	9.53222200	9.54517007	9.55170233
$p=4$	9.55827400	9.55827400	9.55827400	9.55827400	9.55827400
$p=5$	9.55827400	9.55827400	9.55827400	9.55827400	9.55827400
$p=6$	9.55827400	9.55827400	9.55827400	9.55827400	9.55827400
	Speed				
$p=1$	−0.32349136	−0.32189521	−0.32109850	−0.32070049	−0.32050157
$p=2$	−0.32030389	−0.32030300	−0.32030278	−0.32030273	−0.32030271
$p=3$	−0.36396608	−0.34268118	−0.33163562	−0.32600603	−0.32316370
$p=4$	−0.32030271	−0.32030271	−0.32030271	−0.32030271	−0.32030271
$p=5$	−0.32030271	−0.32030271	−0.32030271	−0.32030271	−0.32030271
$p=6$	−0.32030271	−0.32030271	−0.32030271	−0.32030271	−0.32030271

TABLE 4.3

The computed values of the energy (L^2-norm) and speed c of the traveling wave solution, for different time steps and a final time of integration of 30 time units, when $\nu=1/2$, $\delta_3=1$ and $\delta_5=0$, where p is the order of the implicit–explicit BDF scheme.

$\delta_5=0$. The Table depicts computed values of the energy of the solution $E(t)$ defined by

$$E(t) \;=\; \Big(\int_0^{2\pi} \big|u(x,t)\big|^2\,dx\Big)^{1/2} \;=\; \|u(\cdot,t)\|, \tag{4.1}$$

and constant speed c of the traveling wave solutions $u\equiv u(\xi)$, where $\xi=x-ct$. The exact value of c can be found by substituting $u(x,t)=u(\xi)$ in (1.1) and taking the inner product of the resulting equation with u_ξ to give

$$c \;=\; \frac{\int_0^{2\pi} u(\xi)u_x^2(\xi)\,d\xi - \int_0^{2\pi} u_\xi(\xi)\mathcal{D}u(\xi)\,d\xi}{\int_0^{2\pi} u_\xi^2(\xi)\,d\xi}. \tag{4.2}$$

In a transient computation the expression (4.2) with $u(\xi)$ replaced by $u(x,t)$ at a given time t, becomes a spectrally accurate approximation of the traveling-wave speed at large times, as is done in the results presented in Table 4.3. One can easily infer from the results that for $q=1,2,3$, the accuracy in computing these quantities is the same as the accuracy $p=q$ of the scheme (i.e., $|E_k-E_{\text{exact}}|\sim k^p$, where E denotes either the L^2-norm or the speed). For $q=4,5,6$, the relative error is significantly less than 10^{-8} and is too small to be seen in the results presented.

4.2. Numerical integration of the Kawahara equation. In what follows we select certain interesting numerical experiments to illustrate the capabilities of our algorithms and attractor quantification data diagnostic tools. The extensive solution phase-space is characterized by the two independent parameters ν and δ_3 (three in the case of the Benney–Lin equation, including δ_5), and the scope of the present study is

not in the full characterization of the attractors but rather an illustration of certain solutions. A reverse period doubling cascade is presented first, which exhibits the rich dynamical nature of the system, and secondly we compute stable traveling wave solutions that are strongly attractive in the large dispersion limit, $\delta_3 \gg 1$.

Reverse period doubling cascade caused by dispersion. It is well established that as ν decreases the dispersionless Kuramoto–Sivashinsky equation undergoes a period–doubling route to chaos according to the Feigenbaum scenario. For general initial conditions chaos sets in at and beyond the Feigenbaum accumulation point given by $\nu_\infty \approx 0.12122680$, as first shown in [23]. (In the case where the symmetry $u(-x,t) = -u(x,t)$ is imposed, analogous results are found but at smaller values of ν; see [22, 24].) In particular, at the value $\nu = 0.1212 < \nu_\infty$, the solutions at large time are chaotic. In what follows we fix $\nu = 0.1212$ and investigate the effects of dispersion on the underlying dynamics when $\delta_3 > 0$ and $\delta_5 = 0$ in (1.5). Note that without loss of generality we can take δ_3 to be positive since given a solution $u(x,t;\nu,\delta_3)$ then $-u(-x,t;\nu,-\delta_3)$ is also a solution.

Our numerical experiments establish that when δ_3 is sufficiently large ($\delta_3 > 0.073$) the solution enters a traveling wave attractor. Such behavior has been observed by various authors; see, for example, [13, 17, 18]. Of particular interest to us are the dynamics as δ_3 decreases to zero from values that support traveling waves. Starting from $\delta_3 = 0.1$, we observe numerically that at a value $\delta_3 \in (0.07300091, 0.07300092)$ the steady-state traveling wave undergoes its first Hopf bifurcation leading to a traveling time periodic solution, i.e., a solution u satisfying $u(x,t+T) = u(x-\bar{c}t,t)$, where T is the time-period and $\bar{c} = \frac{1}{T}\int_0^T \tilde{c}(t)\,dt$, with $\tilde{c}(t)$ the speed of propagation defined by (see Section 4.1 and equation (4.2) for the derivation of this formula)

$$\tilde{c}(t) \;=\; \frac{\int_0^{2\pi} u(x,t)u_x^2(x,t)\,dx - \int_0^{2\pi} u_x(x,t)\mathcal{D}u(x,t)\,dx}{\int_0^{2\pi} u_x^2(x,t)\,dx}. \tag{4.3}$$

The evolution of $\tilde{c}(t)$ allows us to identify traveling-periodic or traveling wave solutions, with spectral accuracy from knowledge of the Fourier coefficients $a_j(t)$ and $b_j(t)$.

As δ_3 decreases, a series of period doubling bifurcations take place. We followed as many as seven period doublings and estimated the Feigenbaum accumulation point, where chaos sets in, to be $\delta_{3,\infty} \approx 0.00137991$. In Figure 4.2, we depict the phase plane of the energy $(E, \dot{E})$, where

$$\dot{E}(t) \;=\; \frac{\|u_x(\cdot,t)\|^2 - \nu\|u_{xx}(\cdot,t)\|^2}{\|u(\cdot,t)\|}, \tag{4.4}$$

and $E(t)$ has been defined earlier in (4.1). The expression for $\dot{E}(t)$ follows by taking the inner product of (1.1) with $u(\cdot,t)$, and the formula is valid for general dispersion operators. Note also that (4.1) and (4.4) are computed with spectral accuracy since they involve sums in Fourier space. We determine period doublings by tracking the local maxima and minima of $E(t)$ over very long times after transients have died away. For example, in the panel corresponding to $\delta_3 = 0.001385$ (bottom right) there are 32 maxima and minima and the period is $T = 49.182941$. Furthermore, for $\delta_3 = 0.00137992$ we computed an additional five period doublings, so that 1024 maxima and as many minima exist, and the period is $T = 1574.017110030$. In order to isolate such delicate features of the dynamics it is imperative to calculate

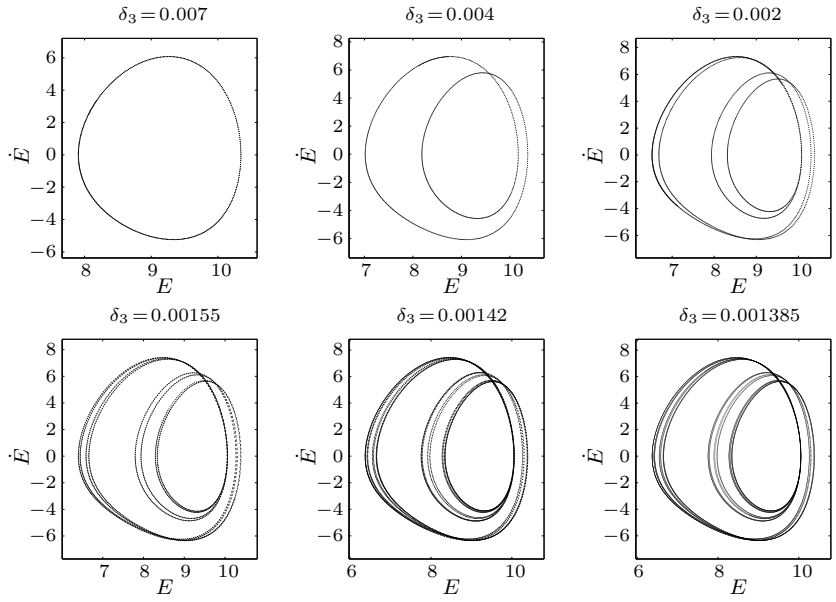

FIG. 4.2. *Phase plane of the L^2-norm. Five period doublings as δ_3 decreases for a fixed $\nu = 0.1212$.*

accurately local maxima and minima (both their values and times of occurrence) and we typically work with twelve decimal places. This is achieved by using weighted polynomial interpolation; in these runs the interpolation fits a sixth degree polynomial to eleven points, with the local extremum in the middle.

For values of δ_3 in the window $[0, \delta_{3,\infty}]$, the dynamics lives on a chaotic attractor. A graphical representation of this chaotic attractor at $\delta = 5 \times 10^{-4}$ is obtained by constructing the return map of the local minima (for example), i.e., by plotting $(\mathfrak{m}_j, \mathfrak{m}_{j+1})$, where $\{\mathfrak{m}_j\}$ is the sequence of the local minimum values as t increases. In Figures 4.3(a)–4.3(b) the foliations in the return map are clearly seen ($\nu = 0.1212$ and $\delta_3 = 5 \times 10^{-4}$); panel (b) is an enlargement of the boxed region in (a). Such self–similar features can only be constructed by integrating to long times in order to allow different parts of the attractor to be visited by the flow. In the present case, the equation was integrated for 10^5 time units with time step $k = 10^{-4}$. Foliations and self–similarity of the attractor are strongly evident in these results, and such qualitative behavior has also been established by the authors in computations of the KS equation and systems of KS type ([4, 22, 23, 24]).

The high dispersion limit: Stable traveling wave attractors. As the value of δ_3 is increased the solutions are attracted to nonlinear traveling waves. Depending on the initial conditions, the traveling waves can have different fundamental periods (or different modal behavior in our description) $2\pi/M$, where M is a positive integer. In the results that follow we have opted to describe attractors with $M = 1$, that is unimodal waves. Three notable generic features emerge from the computations as illustrated in Table 4.4, which provides the effect of δ_3 on the L^2-norm, speed c and asymmetry parameter χ defined by $\chi = \frac{\|u-\tilde{u}\|}{\|u\|}$, where $\tilde{u}(x) = u(-x)$ and $\|u\|$ is the L^2-norm. Both the L^2-norm and the speed increase linearly (asymptotically) with δ_3, whereas the asymmetry parameter χ tends to zero asymptotically indicating that

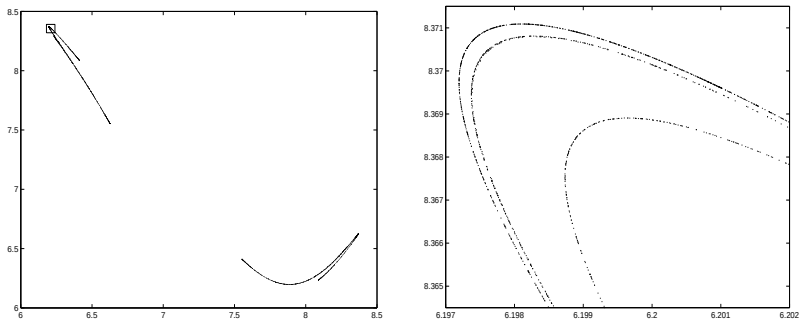

(a) (b)

FIG. 4.3. *Return map showing foliations in the chaotic regime when* $\nu = 0.1212$ *and* $\delta_3 = 5 \times 10^{-4}$. *Panel* (b) *is an enlargement of the boxed region in* (a).

the solutions become increasingly symmetric. These features are easily confirmed by considering a balance of terms in equation 1.4) for $\delta_3 \gg 1$, with the nonlinearity retained in order to provide the required saturation mechanism characteristic of Kuramoto–Sivashinsky type equations. Thus we write

$$u(x,t) = \delta_3 U(x,\tau), \qquad t = \frac{\tau}{\delta_3}, \tag{4.5}$$

where τ is the new scaled time, and substitute into (1.4) to find

$$U_\tau + UU_x + U_{xxx} = -\frac{1}{\delta_3}(U_{xx} + \nu U_{xxxx}). \tag{4.6}$$

Equation (4.6) is a perturbed KdV equation when δ_3 is large and its solutions (traveling wave solutions emerge by writing $U \equiv U(x - s\tau)$ in the usual way) are KdV cnoidal waves perturbed by the Kuramoto–Sivashinsky term on the right of (4.6). A detailed analysis of such limiting traveling waves has been carried out in [13] and additional results will be reported by the authors in future work. The scalings (4.5) clearly show the asymptotic results $\|u(\cdot,t)\| = \mathcal{O}(\delta_3)$ and $c = \mathcal{O}(\delta_3)$ (note that the scaled speed s is given by $s = c/\delta_3$).

δ_3	0.1	0.4	1.6	6.4	25.6	102.4
$\|u\|/\delta_3$	75.0485	28.1913	18.2486	16.9548	16.8543	16.8531
c/δ_3	11.8228	3.9593	2.2071	1.9659	1.9478	1.9466
χ	0.4721	0.3606	0.1646	0.04662	0.01178	0.002946

TABLE 4.4

Variation with the dispersion coefficient δ_3 *of the* L^2-*norm, the speed and the asymmetry parameter* χ *indicating linear asymptotic behavior for the former two quantities and an asymptotically symmetric solution since* χ *decreases to zero. Here,* $\nu = 0.2$.

Finally, we present some computed traveling wave solutions at different values of δ_3 with fixed $\nu = 0.2$. We note that all solutions are stable to perturbations with wavelengths at most as big as the computational domain (of length 2π here),

in the sense that they are computed by solving initial value problems (the possibility of modulational instabilities, i.e., perturbations of larger wavelength than the basic period of the waves, needs to be investigated further). Results are shown in Figure 4.4 with the scaled solutions u/δ_3 collectively depicted in the right panel. The profiles are shifted horizontally (admissible due to Galilean invariance) so that the first term of the solution's Fourier series contains $\cos(x)$ alone (this is done efficiently in Fourier space). It is seen that the solution is converging to a unimodal traveling wave with the self-similar properties outlined earlier, and the symmetry in the asymptotic state also manifests itself.

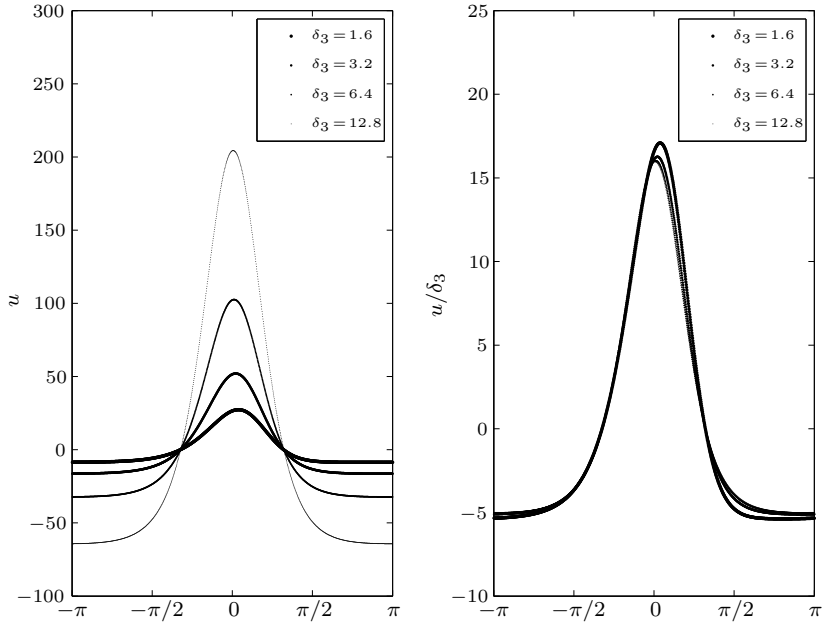

FIG. 4.4. *Traveling waves as δ_3 increases for fixed $\nu = 0.2$. The right panel shows the scaled solution divided by δ_3. Integration was carried out to $t = 15$ to ensure the solution reaches its final state.*

4.3. Numerical integration of Benney–Lin equation. In this section we illustrate our numerical methods for the Benney–Lin equation (1.5) by taking $\delta_3 = 0$ and computing solutions as δ_5 varies. As shown in Section 2, the linearly implicit schemes of order $p = 1, 2$ are appropriate due to the high order dispersion and all results that follow use $p = 2$. As for the Kawahara equation, a sufficient amount of dispersion produces stable traveling wave attractors. The profiles become asymptotically symmetric as δ_5 increases and the L^2-norms and traveling wave speeds grow linearly with δ_5. This is also the case for any dispersive operator $\mathcal{D} \equiv \delta_{\mathcal{D}}\mathcal{D}_1$ in (1.1) and follows by balancing terms after writing $u = \delta_{\mathcal{D}}U$, taking $\delta_{\mathcal{D}} \gg 1$ and proceeding as in Section 4.2. For brevity we do not include quantitative details of these linear variations of the L^2-norm and speed with δ_5, but in Figure 4.5 provide a sequence of stable traveling wave solutions as δ_5 increases for the case $\nu = 0.4$. Twelve values $\delta_5 = 2^m$ are used with $m = -4, -3, \ldots, 6, 7$, and the initial value problem is solved until the emergence of steady-state traveling waves (typically the computation is stopped after the L^2-norm of the solution has converged to at least eight deci-

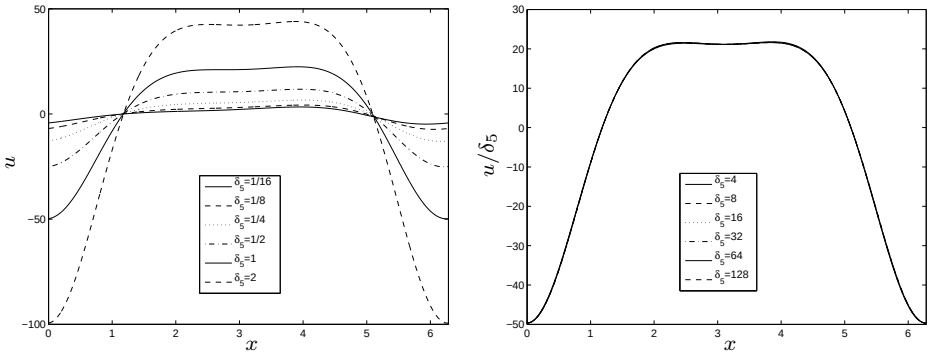

(a) (b)

FIG. 4.5. *Traveling waves for* $\nu = 0.4$*:* (a) *Unscaled solutions for* $\delta_5 = 1/16$, $1/8$, $1/4$, $1/2$, 1, 2*;* (b) *scaled solutions* u/δ_5 *for* $\delta_5 = 4$, 8, 16, 32, 64, 128. *Integration was carried out to* $t = 20$ *for the results in panel* (a) *and* $t = 35$ *for those in panel* (b).

mals). Panel (a) shows the solutions for $\delta_5 = 1/16, 1/8, 1/4, 1/2, 1, 2$ while panel (b) depicts the profiles at the larger values of $\delta_5 \geq 4$. The solutions in panel (b) are plotted after applying the rescaling $U_{\delta_5} = u/\delta_5$ for each value of δ_5 computed, and the superimposed curves are almost indistinguishable (there are six solutions in the figure which have amplitudes that vary by two orders of magnitude). In addition, the solutions become asymptotically symmetric about $x = \pi$ as mentioned earlier, and this fact is useful in the analysis of the equations, which will be reported by the authors elsewhere.

Finally we take $\nu = 0.1$, which supports chaotic solutions in the dispersionless KS equation and compute the attractors as δ_5 decreases. We have established that if δ_5 is larger than or equal to $\delta_{5c} = 0.00366$ the solutions of (1.5) are attracted to a stable bimodal traveling wave attractor. As δ_5 is decreased below δ_{5c} the solution undergoes a sequence of bifurcations leading to chaotic dynamics. Our numerical schemes and numerical diagnostic tools are capable of describing the dynamics qualitatively and quantitatively. In the results that follow we use 40 modes and a step-size $k = 10^{-4}$ with the final time of integration varied appropriately as the parameter δ_5 changes to ensure that no transients are present and the numerical solutions reproduce faithfully the inertial manifold. The route to chaos does not follow a Feigenbaum scenario in this case as opposed to the Kawahara equation computed in Section 4.2. We believe that this is due to the smaller value of $\nu = 0.1$ that was chosen to illustrate the intricate nature of the underlying attractor. As δ_5 decreases chaos emerges through quasi-periodic dynamics in time as described next. A Hopf bifurcation leading to a time periodic solution of period $T = 0.859168$ (correct to six decimals) takes place at $\delta_5 = 0.00365$. This time-periodic attractor persists until approximately $\delta_5 = 0.0030265$ where the period is $T = 0.838348$, with T decreasing monotonically but weakly with δ_5. A further decrease of δ_5 to the value 0.0030264 produces quasi-periodic dynamics in time; another Hopf bifurcation takes place with a small second frequency (approximately 0.00159), inducing modulated dynamics that vary on a second long period, T_2 say, given by $T_2 \approx 3951$. We quantify quasi-periodic dynamics by considering the evolution of the energy minima (or maxima); if the solution is periodic of period T the resulting plot is a series of points lying on a horizontal line (if the energy has one maximum and one minimum as is the case here), and spaced T units apart. When a

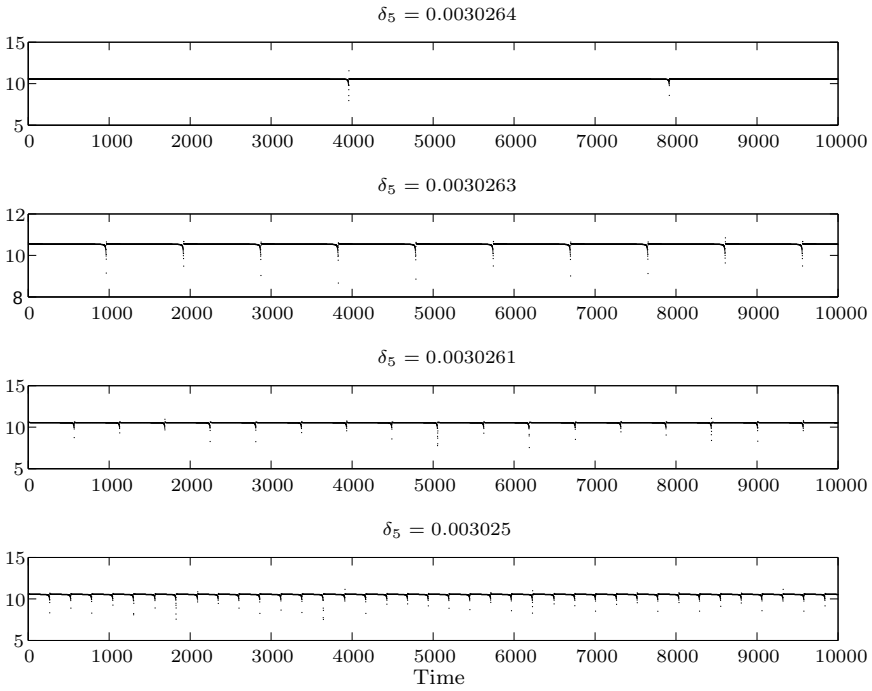

FIG. 4.6. *Quasi-periodic dynamics prior to transition to chaos when* $\nu = 0.1$. *The evolution of the local minima of* $E(t)$ *are plotted as dots as* δ_5 *decreases from* .0030264 *to* .003025 - *values shown in the figure. The average times between "bursts" corresponding to the second period of oscillation, are tabulated in Table 4.5 and decrease monotonically with* δ_5.

second frequency enters, the discrete set of points no longer lie on a straight line but instead the locus of the points is a curve with periodic features as shown in Figure 4.6. The four panels depict solutions for $\delta_5 = 0.0030264, 0.0030263, 0.0030261, 0.003025$ over 10^4 time units and show clearly the dramatic decrease in the second period T_2. The second period is estimated directly from the data and values for a range of δ_5 are given in Table 4.5. (We note that additional evidence of quasi-periodic dynamics is gained by considering return maps of the minima which produce curves in $\mathbb{R}^2$ that fill out as time increases, in analogy with quasi-periodic flow on a torus, for example - for brevity we do not include such plots here.) At lower values of δ_5 a third frequency enters (seen in preliminary runs), which then leads the dynamics into the chaotic regime - the return maps now contain foldings and self-similar features. A complete identification of the third frequency would involve the spectral analysis of long time-series data (of the L^2-norm for instance) and is beyond our purposes here but will be addressed in future work.

δ_5	0.0030264	0.0030263	0.0030262	0.0030261	0.003026	0.003025
T_2	3951	956	688	561	483	260

TABLE 4.5

Quasi-periodic solutions just before the chaotic attractor, $\nu = 0.1$. *Estimates of the values of the second period* T_2 *as* δ_5 *decreases. At* $\delta_5 = 0.0030265$ *the flow is periodic of period* $T = 0.838348$.

5. Conclusions. In this paper we have analyzed and implemented numerical schemes to solve dispersively modified Kuramoto–Sivashinsky equations. Time stepping is achieved using a class of implicit-explicit multistep schemes and spatial discretizations are done spectrally. Optimal order error estimates are derived for general dispersive modifications of the KS equation. Schemes of arbitrary order p can be applied when the number of spatial derivatives of the dispersive term is less than four (this also holds for pseudo-differential operators whose Fourier symbol satisfies analogous sub-dominance conditions), and as a test case we implement these for the Kawahara equation (1.4) for $p = 1, \ldots, 6$. For dispersive operators whose order is higher than four (e.g., the Benney–Lin equation (1.5)), we prove optimal error estimates for the $p = 1, 2$ schemes. These schemes are also implemented and used to illustrate the dynamics of this equation by constructing parts of the underlying attractors. The schemes are found to be an appropriate numerical tool that can be used to faithfully reproduce the dissipative dynamics and attractors.

Extensive runs have been performed that show that dispersion (even in moderate amounts) modifies the inertial manifold in the sense that solutions are attracted to nonlinear traveling waves. In all cases computed limiting traveling wave attractors are found which are independent of the dispersion coefficient and depend on ν alone. We have also implemented several numerical diagnostic tools such as the highly accurate construction of return maps (i.e., the projection of the infinite–dimensional dynamics to a discrete map) that are essential in the discovery and characterization of the attractors. Using these tools we have explored the effect of dispersion on the dispersionless Feigenbaum routes to chaos familiar for the KS. Starting with a value of ν in the chaotic regime just beyond the Feigenbaum accumulation point ν_∞ (see definitions in the main text), we show that if the dispersion is sufficiently large then the solution is attracted to a traveling wave. Our computations show that a reduction in the dispersion leads to chaos through a Feigenbaum period–doubling cascade - see Section 4.2. The dispersion acts in a stabilizing manner in the sense that the Feigenbaum period–doubling cascade is delayed to lower values of ν and takes place with respect to the second parameter in the problem, the dispersion coefficient δ_3 in the case of the Kawahara equation. In the case of the Benney–Lin equation (1.5) that contains a fifth order dispersive term, our computations using the $p = 2$ scheme again indicate the existence of high dispersion limiting stable traveling wave attractors. We have also illustrated the dynamics as the dispersion decreases for the value $\nu = 0.1$, and find a quasi–periodic route to chaos: two Hopf bifurcations produce quasi–periodic dynamics before chaos ensues most probably due to a third frequency that enters. Additional work is under way to clarify this scenario using the numerical methods described and analyzed here.

REFERENCES

[1] G. Akrivis and M. Crouzeix, *Linearly implicit methods for nonlinear parabolic equations*, Math. Comp. **73** (2004) 613–635.

[2] G. Akrivis, M. Crouzeix, and Ch. Makridakis, *Implicit–explicit multistep finite element methods for nonlinear parabolic problems*, Math. Comp. **67** (1998) 457–477.

[3] G. Akrivis, M. Crouzeix, and Ch. Makridakis, *Implicit–explicit multistep methods for quasi-linear parabolic equations*, Numer. Math. **82** (1999) 521–541.

[4] G. Akrivis, D. T. Papageorgiou, and Y.-S. Smyrlis, *Linearly implicit methods for a semilinear parabolic system arising in two–phase flows*, IMA J. Numer. Anal. **31** (2011) 299–321.

[5] G. Akrivis, D. T. Papageorgiou, and Y.-S. Smyrlis, *Linearly implicit spectral schemes for the dispersively modified Kuramoto–Sivashinsky equations*, Technical Report, 2010.

[6] G. Akrivis and Y.-S. Smyrlis, *Implicit–explicit BDF spectral methods for the Kuramoto–Sivashinsky equation*, Appl. Numer. Math. **51** (2004) 151–169.
[7] G. Akrivis and Y.-S. Smyrlis, *Linearly implicit schemes for a class of dispersive–dissipative systems*, Calcolo **48** (2011) 145–172.
[8] D. J. Benney, *Long waves on liquid films*, J. Math. and Phys. **45** (1966) 150–155.
[9] C. Bernardi and Y. Maday, *Spectral methods.* In Handbook of Numerical Analysis, Vol. V, Techniques of Scientific Computing (Part 2), (P. G. Ciarlet & J. L. Lions, eds). Elsevier, Amsterdam, 1997, pp. 209–486.
[10] H. A. Biagioni and F. Linares, *On the Benney–Lin and Kawahara equations*, J. Math. Anal. Appl. **211** (1997) 131–152.
[11] C. Canuto, M. Y. Hussaini, A. Quarteroni and T. A. Zang, *Spectral Methods in Fluid Dynamics*, Springer–Verlag, New York, Springer Series in Computational Physics, 1988.
[12] P. Collet, J.-P. Eckmann, H. Epstein and J. Stubbe, *Analyticity for the Kuramoto–Sivashinsky equation*, Physica D **67** (1993) 321–326.
[13] N.M. Ercolani, D.W. McLaughlin and H. Roitner, *Attractors and transients for a perturbed periodic KdV equation*: *A nonlinear spectral analysis*, J. Nonlinear Sci. **3** (1993) 477–539.
[14] A. L. Frenkel and K. Indireshkumar, *Wavy film flows down an inclined plane*: *perturbation theory and general evolution equation for the film thickness*, Phys. Rev. E (3) **60** (1999) 4143–4157.
[15] M. Frankel and V. Roytburd, *Dissipative dynamics for a class of nonlinear pseudo–differential equations*, J. Evol. Equ. (3), **8** (2008) 491–512.
[16] S. Kas–Danouche, D. T. Papageorgiou, and M. Siegel, *Nonlinear dynamics of core-annular film flows in the presence of surfactant*, J. Fluid Mech. **626** (2009) 415–448.
[17] T. Kawahara, *Formation of saturated solitons in a nonlinear dispersive system with instability and dissipation*, Phys. Rev. Lett. **51** (1983) 381–382.
[18] T. Kawahara and S. Toh, *Nonlinear dispersive waves in the presence of instability and damping*, Phys. Fluids **28** (1985) 1636–1638.
[19] T. Kawahara and S. Toh, *On some properties of solutions to a nonlinear evolution equation including long–wavelength instability*, Nonlinear wave motion, Pitman Monogr. Surveys Pure Appl. Math., 43, pp. 95–117, Longman Sci. Tech., Harlow, 1989.
[20] S. P. Lin, *Finite amplitude side–band stability of a viscous film*, J. Fluid Mech. **63** (1974) 417–429.
[21] D. T. Papageorgiou, C. Maldarelli, and D. S. Rumschitzki, *Nonlinear interfacial stability of cone-annular film flow*, Phys. Fluids **A2** (1990) 340–352.
[22] D. T. Papageorgiou and Y.-S. Smyrlis, *The route to chaos for the Kuramoto-Sivashinsky equation*, Theoret. Comput. Fluid Dynamics **3** (1991) 15–42.
[23] D. T. Papageorgiou, and Y.-S. Smyrlis, *Computational study of chaotic and ordered solutions of the Kuramoto–Sivashinsky equation*, NASA Contractor Report 198283, ICASE Report No. 96–12, February 1996.
[24] Y.–S. Smyrlis and D. T. Papageorgiou, Predicting chaos for infinite–dimensional dynamical systems: the Kuramoto–Sivashinsky equation, a case study, *Proc. Nat. Acad. Sci. U.S.A.* **88** (1991) 11129–11132.
[25] E. Tadmor *The well–posedness of the Kuramoto–Sivashinsky equation,* SIAM J. Math. Anal. **17** (1986) 884–893.
[26] J. Topper and T. Kawahara, *Approximate equations for long nonlinear waves on a viscous fluid*, J. Phys. Soc. Japan **44** (1978) 663–666.